Highly Luminescent Tris(β-diketonate)europium(III) Complexes Immobilized in a Functionalized Mesoporous Silica

Sandra Gago,[†] José A. Fernandes,[†] José P. Rainho,[‡] Rute A. Sá Ferreira,[‡] Martyn Pillinger,[†] Anabela A. Valente,[†] Teresa M. Santos,[†] Luís D. Carlos,*[,‡] Paulo J. A. Ribeiro-Claro,[†] and Isabel S. Gonçalves*[,†]

Department of Chemistry, and Department of Physics, CICECO, University of Aveiro, 3810-193 Aveiro, Portugal

Received July 4, 2005

The mesoporous silica MCM-41 functionalized with a chelating pyrazolylpyridine ligand (MCM-41-L2) was used as a support for the immobilization of tris(β-diketonate) complexes $Ln(NTA)_3$ [Ln = Eu, Gd; NTA = 1-(2-naphthoyl)-3,3,3-trifluoroacetonate]. The derivatized materials were characterized by powder X-ray diffraction, N_2 adsorption, FTIR and FT Raman spectroscopy, Eu L_3-edge X-ray absorption fine structure (XAFS), diffuse reflectance, and photoluminescence spectroscopy. The spectroscopic studies, supported by ab initio calculations, provide strong evidence that the immobilized europium(III) complex is 8-coordinate, with a local coordination environment that is similar to that for a model complex containing the ligand ethyl[3-(2-pyridyl)-1-pyrazolyl]acetate (L1). No emission from the pyrazolylpyridine ligands is observed in the room-temperature emission spectrum of MCM-41-L2/Eu, despite the fact that only about one-third are engaged in coordination with Eu^{3+} ions. In contrast, the pyrazolylpyridine groups in the precursor ligand-silica exhibit efficient emission. Furthermore, the radiance value measured for MCM-41-L2/ Eu (0.33 μW cm^{-2}) is only about one-half of that measured for the complex $Eu(NTA)_3$·L1 (0.73 μW cm^{-2}), even though the concentration of emitting centers in the MCM material is much lower. The results point to the existence of an unusual two-step intermolecular energy transfer between "free" and complexed ligands in MCM-41-L2/Eu, culminating in the observation of enhanced Eu^{3+} luminescence.

Introduction

The trivalent cations of the lanthanides have photoluminescence properties that are favorable for a broad range of optical applications such as fiber amplifiers and solid-state lasers.[1] However, it is difficult to generate this luminescence by direct excitation of the lanthanide ion, because the absorption bands are weak and narrow. To enhance absorption, lanthanide ions are chelated with organic ligands that have broad, intense absorption bands.[2] The metal-centered luminescence originates from the intramolecular energy transfer through the excited state of the ligand to the emitting level of the lanthanide ion. This is the so-called "antenna effect".[3] Some of the best ligands for these purposes are β-diketonates bearing aromatic and fluorine substituents.[2] For example, the experimental quantum yield measured for $Eu(NTA)_3$·2DMSO [NTA = 1-(2-naphthoyl)-3,3,3-trifluoroacetonate; DMSO = dimethyl sulfoxide], 0.75, is one of the highest so far reported for solid-state europium complexes.[4] The formation of coordinatively saturated complexes is important because it prevents the approach of solvent molecules containing O−H groups, which can quench the luminescence by the nonradiative dissipation of energy on the high-energy O−H vibrations. Apart from monodentate ligands such as DMSO, heterocyclic amines such as 2,2′-bipyridine and 1,10-phenanthroline have been extensively studied as adducting molecules.[5]

The practical application of lanthanide chelate complexes in optical devices is limited to a large extent by their poor thermal stability and low mechanical strength. One solution is to immobilize the complexes in a stable rigid matrix, for

* To whom correspondence should be addressed. I.S.G.: (tel.) 00351-234-378190; (fax) 00351-234-370084; (e-mail) igoncalves@dq.ua.pt. L.D.C.: (tel.) 00351-234-370946; (fax) 00351-234-424965; (e-mail) lcarlos@fis.ua.pt.

[†] Department of Chemistry.

[‡] Department of Physics.

(1) Jüstel, T.; Nikol, H.; Ronda, C. *Angew. Chem., Int. Ed.* **1998**, *37*, 3084.

(2) (a) Lis, S.; Elbanowski, M.; Mąkowska, B.; Hnatejko, Z. *J. Photochem. Photobiol.* **2002**, *150*, 233. (b) de Sá, G. F.; Malta, O. L.; de Mello Donegá, C.; Simas, A. M.; Longo, R. L.; Santa-Cruz, P. A.; da Silva, E. F., Jr. *Coord. Chem. Rev.* **2000**, *196*, 165.

(3) Alpha, B.; Ballardini, R.; Balzani, V.; Lehn, J.-M.; Perathoner, S.; Sabbatini, N. *Photochem. Photobiol.* **1990**, *52*, 299.

(4) Carlos, L. D.; de Mello Donegá, C.; Albuquerque, R. Q.; Alves, S., Jr.; Menezes, J. F. S.; Malta, O. L. *Mol. Phys.* **2003**, *101*, 1037.

(5) (a) Trikha, A. K.; Zinner, L. B.; Zinner, K.; Isolani, P. C. *Polyhedron* **1996**, *15*, 1651. (b) Batista, H. J.; de Andrade, A. V. M.; Longo, R. L.; Simas, A. M.; de Sá, G. F.; Ito, N. K.; Thompson, L. C. *Inorg. Chem.* **1998**, *37*, 3542. (c) Thompson, L. C.; Atchison, F. W.; Young, V. G. *J. Alloys Compd.* **1998**, *275*−*277*, 765. (d) Iftikhar, K.; Sayeed, M.; Ahmed, N. *Inorg. Chem.* **1982**, *21*, 80. (e) Moser, D. F.; Thompson, L. C.; Young, V. G., Jr. *J. Alloys Compd.* **2000**, *303*−*304*, 121. (f) Malta, O. L.; Couto dos Santos, M. A.; Thompson, L. C.; Ito, N. K. *J. Lumin.* **1996**, *69*, 77. (g) Tsaryuk, V.; Legendziewicz, J.; Puntus, L.; Zolin, V.; Sokolnicki, J. *J. Alloys Compd.* **2000**, *300*−*301*, 464. (h) Holz, R. C.; Thompson, L. C. *Inorg. Chem.* **1993**, *32*, 5251. (i) Thompson, L. C.; Berry, S. *J. Alloys Compd.* **2001**, *323*−*324*, 177. (j) Holz, R. C.; Thompson, L. C. *Inorg. Chem.* **1988**, *27*, 4640. (k) Uekawa, M.; Miyamoto, Y.; Ikeda, H.; Kaifu, K.; Nakaya, T. *Bull. Chem. Soc. Jpn.* **1998**, *71*, 2253. (l) Fernandes, J. A.; Sá Ferreira, R. A.; Pillinger, M.; Carlos, L. D.; Jepsen, J.; Hazell, A.; Ribeiro-Claro, P.; Gonçalves, I. S. *J. Lumin.* **2005**, *113*, 50. (m) Fernandes, J. A.; Sá Ferreira, R. A.; Pillinger, M.; Carlos, L. D.; Gonçalves, I. S.; Ribeiro-Claro, P. J. A. *Eur. J. Inorg. Chem.* **2004**, 3913. (n) Bellusci, A.; Barberio, G.; Crispini, A.; Ghedini, M.; La Deda, M.; Pucci, D. *Inorg. Chem.* **2005**, *44*, 1818.

10.1021/cm0514490 CCC: $30.25
Published on Web 09/10/2005

example, a polymer or silica-based material.[6,7] In the past few years, micelle-templated silicas have started to attract attention as mesostructured hosts for optical functionalities, mainly organic dyes and polymers.[8,9] Lanthanide tris- and tetrakis-β-diketonates have also been immobilized in the ordered mesoporous silicas MCM-41 and MCM-48 by simple wet impregnation methods.[10] The mesoporous supports were used either in the purely siliceous form or modified with propylamine, ethylenediamine, and nitrile groups. In these examples, the photophysical properties of the encapsulated rare earth complexes depend greatly on the hydrogen-bonding interactions between the host and the guest. Another interesting, yet largely unexplored, possibility concerns the complexation of lanthanides by ligands that are covalently anchored to the support. The potential advantages of this approach have recently been shown by the coupling of lanthanide β-diketonate complexes to sol−gel glasses and a Merrifield resin via covalently bound 1,10-phenanthroline.[11]

In this paper, we show that lanthanide tris-β-diketonate complexes can be linked covalently to a mesoporous silica by adduct formation with a surface-bound pyrazolylpyridine ligand. We chose to study the $Ln(NTA)_3$ system due to the promising luminescence properties of the europium complexes $Eu(NTA)_3 \cdot L$.[5l] A hybrid ligand-silica derivatized with a pyrazolylpyridine ligand was selected as the support because it is straightforward to prepare and has already been shown to successfully bind molybdenum and manganese complexes.[12] The spectroscopic studies confirm the successful tethering of coordinatively saturated complexes and point to the existence of an unusual two-step intermolecular energy transfer between "free" and complexed ligands, which culminates in the observation of enhanced Eu^{3+} luminescence.

Experimental Section

Characterization. Microanalyses were performed at the Instituto de Tecnologia Química e Biológica (by C. Almeida). Room-temperature powder XRD data were collected on a Philips X'pert diffractometer with a curved graphite monochromator (Cu Kα radiation), in a Bragg−Brentano para-focusing optics configuration. Samples were step-scanned in 0.02° 2θ steps with a counting time of 2 s per step. BET specific surface areas (S_{BET}, p/p_0 from 0.03 to 0.13) and specific total pore volumes, V_t, were estimated from N_2 adsorption isotherms measured at 77 K, as described previously.[13] The pore size distributions (PSD) were calculated by the BJH method using the modified Kelvin equation with a correction for the statistical film thickness on the pore walls.[14] The statistical film thickness was calculated using the Harkins−Jura equation in the p/p_0 range from 0.1 to 0.95.

IR spectra were obtained as KBr pellets using a FTIR Mattson-7000 infrared spectrophotometer. Raman spectra were recorded on a Bruker RFS100/S FT instrument (Nd:YAG laser, 1064 nm excitation, InGaAs detector). Ab initio calculations were performed using the G03 program package.[15] The fully optimized geometry, the harmonic vibrational frequencies, and the infrared and Raman intensities were obtained at the B3LYP level, using the Effective Core Potentials of Pacios and Christiansen[16] for the Eu atom and the CEP-4G basis set for the remaining atoms. ^{1}H NMR spectra were measured in solution using a Bruker CXP 300 spectrometer.

Eu L_3-edge X-ray absorption spectra were measured in transmission mode on beamline BM29 at the ESRF (Grenoble),[17] operating at 6 GeV in hybrid mode with typical currents of 170−190 mA. Scans were set up to record the pre-edge at 5 eV steps and the post-edge region in 0.025−0.05 Å^{-1} steps, giving a total acquisition time of ca. 30 min per scan. Harmonic rejection was achieved by detuning the order-sorting double Si(311) crystal monochromator by 50%. Solid samples were diluted with BN and pressed into 13 mm pellets. Ionization chamber detectors were filled with N_2 to give 30% absorbing I_o (incidence) and 70% absorbing I_t (transmission). The programs EXCALIB and EXBACK (SRS Daresbury Laboratory, UK) were used in the usual manner for calibration and background subtraction of the raw data. EXAFS curve-fitting analyses, by least-squares refinement of the non-Fourier filtered k^3-weighted EXAFS data, were carried out using the program EXCURVE (version EXCURV98[18]) using fast curved wave theory.[19] The calculations were performed with single scattering contributions only. Phase shifts were obtained within this program using ab initio calculations based on the Hedin Lundqvist/von Barth scheme. For each EXAFS simulation, the validity of extra parameters was checked using a comparative reduced χ^2 method.[20]

(6) (a) Sanchez, C.; Lebeau, B.; Chaput, F.; Boilot, J. P. *Adv. Mater.* **2003**, *15*, 1969. (b) Kuriki, K.; Koike, Y.; Okamoto, Y. *Chem. Rev.* **2002**, *102*, 2347. (c) Maas, H.; Currao, A.; Calzaferri, G. *Angew. Chem., Int. Ed.* **2002**, *41*, 2495. (d) Sendor, D.; Kynast, U. *Adv. Mater.* **2002**, *14*, 1570.

(7) (a) Hernandez, R.; Franville, A.-C.; Minoofar, P.; Dunn, B.; Zink, J. I. *J. Am. Chem. Soc.* **2001**, *123*, 1248. (b) Minoofar, P.; Hernandez, R.; Chia, S.; Dunn, B.; Zink, J. I.; Franville, A.-C. *J. Am. Chem. Soc.* **2002**, *124*, 14388.

(8) (a) Wirnsberger, G.; Stucky, G. D. *ChemPhysChem* **2000**, *1*, 89. (b) Scott, B. J.; Wirnsberger, G.; Stucky, G. D. *Chem. Mater.* **2001**, *13*, 3140.

(9) (a) Molenkamp, W. C.; Watanabe, M.; Miyata, H.; Tolbert, S. H. *J. Am. Chem. Soc.* **2004**, *126*, 4476. (b) Nguyen, T.-Q.; Wu, J.; Doan, V.; Schwartz, B. J.; Tolbert, S. H. *Science* **2000**, *288*, 652. (c) Fukuoka, A.; Miyata, H.; Kuroda, K. *Chem. Commun.* **2003**, 284.

(10) (a) Meng, Q. G.; Boutinaud, P.; Franville, A.-C.; Zhang, H. J.; Mahiou, R. *Microporous Mesoporous Mater.* **2003**, *65*, 127. (b) Fu, L.; Zhang, H.; Boutinaud, P. *J. Mater. Sci. Technol.* **2001**, *17*, 293. (c) Xu, Q.; Li, L.; Liu, X.; Xu, R. *Chem. Mater.* **2002**, *14*, 549.

(11) (a) Binnemans, K.; Lenaerts, P.; Driesen, K.; Görller-Walrand, C. *J. Mater. Chem.* **2004**, *14*, 191. (b) Lenaerts, P.; Driesen, K.; Van Deun, R.; Binnemans, K. *Chem. Mater.* **2005**, *17*, 2148.

(12) (a) Jia, M. J.; Seifert, A.; Thiel, W. R. *Chem. Mater.* **2003**, *15*, 2174. (b) Gago, S.; Zhang, Y.; Santos, A. M.; Köhler, K.; Kühn, F. E.; Fernandes, J. A.; Pillinger, M.; Valente, A. A.; Santos, T. M.; Ribeiro-Claro, P. J. A.; Gonçalves, I. S. *Microporous Mesoporous Mater.* **2004**, *76*, 131.

(13) Nunes, C. D.; Pillinger, M.; Valente, A. A.; Gonçalves, I. S.; Rocha, J.; Ferreira, P.; Kühn, F. E. *Eur. J. Inorg. Chem.* **2002**, 1100.

(14) (a) Kruk, M.; Jaroniec, M.; Sayari, A. *Langmuir* **1997**, *13*, 6267. (b) Kruk, M.; Antochshuk, V.; Jaroniec, M. *J. Phys. Chem. B* **1999**, *103*, 10670.

(15) Frisch, M. J.; Trucks, G. W.; Schlegel, H. B.; Scuseria, G. E.; Robb, M. A.; Cheeseman, J. R.; Zakrzewski, V. G.; Montgomery, J. A.; Stratmann, R. E.; Burant, J. C.; Dapprich, S.; Millam, J. M.; Daniels, A. D.; Kudin, K. N.; Strain, M. C.; Farkas, O.; Tomasi, J.; Barone, V.; Cossi, M.; Cammi, R.; Mennucci, B.; Pomelli, C.; Adamo, C.; Clifford, S.; Ochterski, J.; Petersson, G. A.; Ayala, P. Y.; Cui, Q.; Morokuma, K.; Malick, D. K.; Rabuck, A. D.; Raghavachari, K.; Foresman, J. B.; Cioslowski, J.; Ortiz, J. V.; Stefanov, B. B.; Liu, G.; Liashenko, A.; Piskorz, P.; Komaromi, I.; Gomperts, R.; Martin, R. L.; Fox, D. J.; Keith, T.; Al-Laham, M. A.; Peng, C. Y.; Nanayakkara, A.; Gonzalez, C.; Challacombe, M.; Gill, P. M. W.; Johnson, B. G.; Chen, W.; Wong, M. W.; Andres, J. L.; Head-Gordon, M.; Replogle, E. S.; Pople, J. A. *Gaussian 98*, revision A.1; Gaussian, Inc.: Pittsburgh, PA, 1998.

(16) Pacios, L. F.; Christiansen, P. A. *J. Chem. Phys.* **1985**, *82*, 2664.

(17) Filipponi, A.; Borowski, M.; Bowron, D. T.; Ansell, S.; Cicco, A. D.; Panfilis, S. D.; Itiè, J.-P. *Rev. Sci. Instrum.* **2000**, *71*, 2422.

(18) Binsted, N. Excurv98, CCLRC Daresbury Laboratory computer program, 1998.

(19) (a) Gurman, S. J.; Binsted, N.; Ross, I. *J. Phys. C* **1984**, *17*, 143. (b) Gurman, S. J.; Binsted, N.; Ross, I. *J. Phys. C* **1986**, *19*, 1845.

(20) O'Donnell, K. P.; Mosselmans, J. F. W.; Martin, R. W.; Pereira, S.; White, M. E. *J. Phys.: Condens. Matter* **2001**, *13*, 6977.

Room-temperature emission and excitation photoluminescence spectra and lifetime measurements were recorded on a modular double grating excitation spectrofluorimeter (Fluorolog-3, Jobin Yvon-Spex) with a TRIAX 320 emission monochromator coupled to a R928 Hamamatsu photomultiplier, in the front-face acquisition mode. All of the photoluminescence spectra were corrected for optics and detection spectral response. The luminance measurements were obtained using a telescope optical probe (TOP 100 DTS140-111, Instrument Systems). The excitation source was a Xe arc lamp (150 W) coupled to a Jobin Yvon-Spex monochromator (TRIAX 180). The width of the rectangular excitation spot was set as 2 mm, and the diameter used to collect the emission intensity was smaller (0.5 mm) to ensure that the entire sample was illuminated. As a reference, the radiance of the red phosphor Y_2O_3:Eu (Phosphor Technology) was also measured for a 260 nm excitation wavelength. For all of the measurements, the experimental conditions were kept constant to enable the quantitative comparison between the measurements.

Synthesis. Literature procedures were used to prepare the compounds $Ln(NTA)_3 \cdot 2H_2O$ (Ln = Eu, Gd),[21] the ligands ethyl-[3-(2-pyridyl)-1-pyrazolyl]acetate (L1)[22] and (3-triethoxysilylpropyl)[3-(2-pyridyl)-1-pyrazolyl]acetamide (L2),[12a] and MCM-41 grafted with L2 (MCM-41-L2).[12] Elemental analysis, FTIR, FT Raman, and ^{13}C CP MAS NMR data for MCM-41-L2 are given in ref 12b. The ^{29}Si MAS and CP MAS NMR spectra were in agreement with that reported.[12a]

Model Compounds. A solution of ethyl[3-(2-pyridyl)-1-pyrazolyl]acetate (0.10 g, 0.43 mmol) in $CHCl_3$ (10 mL) was added to a solution of $Ln(NTA)_3 \cdot 2H_2O$ (0.43 mmol) in $CHCl_3$ (20 mL) at room temperature, and stirring continued for 4 h. The solution was evaporated to dryness, and the resultant solid was washed with diethyl ether and dried in a vacuum.

$Eu(NTA)_3 \cdot L1 \cdot H_2O$ (1). (0.26 g, 50%). $C_{54}H_{37}F_9N_3O_8Eu \cdot H_2O$ requires C, 54.19; H, 3.28; N, 3.51%. Found: C, 54.17; H, 3.00; N, 3.35%. ν_{max}/cm^{-1} 3061 (w), 2991 (w), 1757 (m), 1638 (s), 1610 (vs), 1594 (s), 1569 (s), 1531 (s), 1509 (s), 1475 (m), 1463 (m), 1437 (m), 1354 (m), 1299 (vs), 1251 (m), 1199 (s), 1188 (s), 1133 (s), 1073 (m), 958 (m), 866 (w), 792 (s), 767 (m), 748 (m), 683 (m), 568 (m), 471 (m) (KBr); Raman (cm^{-1}) 3059 (m), 2942 (w), 1623 (s), 1607 (m), 1571 (w), 1595 (m), 1531 (m), 1511 (w), 1466 (s), 1434 (m), 1388 (vs), 1355 (m), 1306 (m), 1290 (m), 1219 (m), 1202 (m), 1147 (w), 1126 (w), 1074 (w), 1056 (w), 1015 (m), 961 (m), 937 (w), 870 (w), 772 (s), 720 (w), 685 (w), 519 (m), 229 (w), 195 (w); δ_H (300 MHz, $CDCl_3$, $SiMe_4$) 12.41 (br, 1H, L1), 12.17 (br, 1H, L1), 10.08 (br, 1H, L1), 9.98 (br, 1H, L1), 9.21 (br, 2H, L1), 7.81 (d, $J = 8$ Hz, 3H, naphth), 7.64 (m, 6H, naphth), 7.46 (m, 9H, naphth), 7.34 (t, $J = 8$ Hz, 3H, naphth), 3.59 (q, $J = 7$ Hz, 2H, CH_2CH_3), 3.12 (s, 3H, COCHCO), 0.75 (t, $J = 7$ Hz, 3H, CH_2CH_3).

$Gd(NTA)_3 \cdot L1 \cdot H_2O$ (2). (0.33 g, 57%). $C_{54}H_{37}F_9N_3O_8Gd \cdot H_2O$ requires C, 53.95; H, 3.27; N, 3.50. Found: C, 53.87; H, 3.19; N, 3.26%. ν_{max}/cm^{-1} 3060 (w), 2992 (w), 1756 (m), 1639 (s), 1611 (vs), 1593 (s), 1570 (s), 1532 (s), 1509 (s), 1477 (m), 1463 (m), 1437 (m), 1385 (w), 1369 (m), 1354 (m), 1301 (vs), 1251 (m), 1199 (s), 1188 (s), 1133 (s), 1073 (m), 958 (m), 866 (m), 793 (s), 767 (m), 748 (m), 684 (m), 569 (m), 519 (m), 471 (m) (KBr); Raman (cm^{-1}) 3059 (m), 2942 (w), 2878 (w), 1623 (s), 1608 (m), 1571 (m), 1595 (m), 1532 (m), 1511 (w), 1466 (s), 1434 (m), 1388 (vs), 1355 (m), 1306 (m), 1290 (m), 1219 (m), 1201 (m), 1147 (w), 1127 (w), 1074 (w), 1056 (w), 1015 (m), 961 (m), 937 (w), 870 (w), 772 (s), 720 (w), 685 (w), 519 (m), 230 (w), 195 (w).

(21) Charles, R. G.; Perrotto, A. *J. Inorg. Nucl. Chem.* **1964**, *26*, 373.
(22) Thiel, W. R.; Angstl, M.; Priermeier, T. *Chem. Ber.* **1994**, *127*, 2373.

Scheme 1. Synthesis of the Model Complexes $Ln(NTA)_3 \cdot L1$ and the Supported Materials MCM-41-L2/Ln

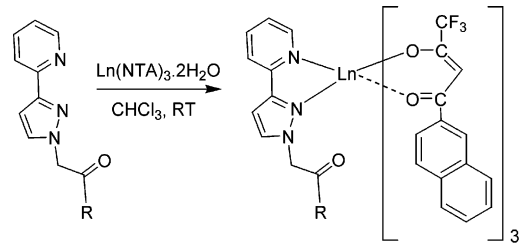

L1: R = $-OCH_2CH_3$ L1: Ln = Eu (**1**), Gd (**2**)
L2: R = $-NH(CH_2)_3Si$-MCM-41 L2: MCM-41-L2/Ln (Ln = Eu, Gd)

Lanthanide-Doped Hybrids. A solution of $Ln(NTA)_3 \cdot 2H_2O$ (0.43 mmol) in $CHCl_3$ (15 mL) was added to a suspension of MCM-41-L2 (0.72 g) in $CHCl_3$ (15 mL). The mixture was stirred at room temperature for 24 h. The pale yellow solid was then filtered, washed several times with $CHCl_3$, and dried in a vacuum. The excess $Ln(NTA)_3 \cdot 2H_2O$ was recovered from the washings (0.30 mmol for MCM-41-L2/Eu and 0.34 mmol for MCM-41-L2/Gd).

MCM-41-L2/Eu. Found: C, 14.12; H, 2.10; N, 2.20; Eu, 2.0%. ν_{max}/cm^{-1} 3431 (br), 2985 (w), 2942 (sh), 1617 (m), 1570 (w), 1534 (w), 1508 (w), 1464 (w), 1436 (w), 1384 (w), 1363 (w), 1299 (w), 1226 (sh), 1080 (vs), 959 (m), 794 (s), 684 (w), 569 (w), 458 (vs); Raman (cm^{-1}) 3148 (w), 3068 (m), 2978 (w), 2936 (m), 2898 (w), 1628 (s), 1599 (s), 1570 (w), 1528 (w), 1468 (s), 1431 (w), 1404 (w), 1385 (vs), 1355 (w), 1299 (s), 1229 (w), 1197 (w), 1150 (w), 1130 (w), 1094 (w), 1053 (w), 1008 (m), 962 (m), 937 (w), 869 (w), 796 (w), 770 (m), 684 (w), 517 (w), 390 (w), 305 (w), 228 (w), 189 (w).

MCM-41-L2/Gd. Found: C, 13.28; H, 2.29; N, 2.07; Gd, 1.2%. ν_{max}/cm^{-1} 3426 (br), 2986 (w), 2946 (sh), 1618 (w), 1570 (w), 1535 (w), 1509 (w), 1499 (w), 1463 (w), 1433 (w), 1405 (w), 1384 (w), 1363 (w), 1299 (w), 1202 (sh), 1078 (vs), 958 (m), 795 (s), 685 (w), 568 (w), 460 (vs). Raman (cm^{-1}) 3147 (w), 3065 (m), 2980 (w), 2936 (m), 2898 (w), 1630 (s), 1602 (s), 1573 (m), 1529 (vs), 1498 (w), 1469 (s), 1446 (w), 1432 (w), 1406 (w), 1386 (vs), 1366 (w), 1302 (m), 1230 (w), 1198 (w), 1151 (w), 1129 (w), 1096 (w), 1054 (w), 1010 (m), 963 (m), 936 (w), 870 (w), 795 (w), 770 (m), 686 (w), 631 (w), 517 (m), 393 (w), 308 (w), 228 (w), 185 (w), 118 (w).

Results and Discussion

Synthesis. Model compounds containing the ligand ethyl-[3-(2-pyridyl)-1-pyrazolyl]acetate (L1) were prepared by the reaction of $Ln(NTA)_3 \cdot 2H_2O$ (Ln = Eu, Gd) with 1 equiv of the ligand L1 (Scheme 1). The supported materials MCM-41-L2/Ln were prepared in a similar way by treatment of MCM-41-L2 with an excess of $Ln(NTA)_3 \cdot 2H_2O$ in chloroform. Elemental analysis indicated that the europium loading in MCM-41-L2/Eu (2.0 wt %) was ca. 34% of the ligand (L2) content, while in MCM-41-L2/Gd the gadolinium loading (1.2 wt %) was ca. 21% of the ligand content. These values were consistent with the recovered quantities of the reagents $Ln(NTA)_3 \cdot 2H_2O$.

Powder XRD and N_2 Adsorption. Figure 1 shows the powder XRD patterns for the pristine calcined MCM-41 starting material, MCM-41-L2, and MCM-41-L2/Eu. The unmodified MCM-41 sample exhibits five reflections in the 2θ range 2−8°, indexed for a hexagonal cell as (100), (110), (200), (210), and (300). The d value of the (100) reflection is 35.8 Å, and the lattice constant $a = 41.4$ Å ($=2d_{100}/\sqrt{3}$).

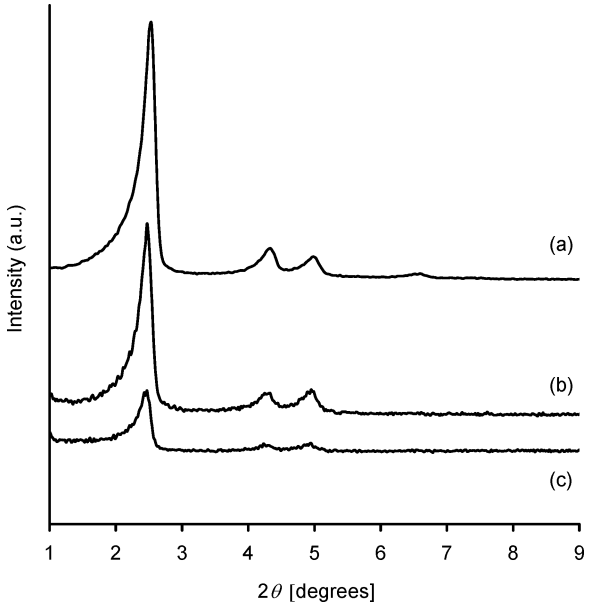

Figure 1. Powder XRD patterns of pristine calcined MCM-41 (a), MCM-41-L2 (b), and MCM-41-L2/Eu (c).

Upon functionalization of MCM-41 and subsequent inclusion of the europium complex, the characteristic reflections are still observed at about the same positions, demonstrating that the long-range hexagonal symmetry of the mesoporous host was preserved. The attenuation of the X-ray peaks, especially after inclusion of the bulky europium complex, is not interpreted as a loss of crystallinity but rather to a reduction in the X-ray scattering contrast between the silica walls and pore-filling material.[23]

The original MCM-41 sample exhibited a reversible type IV nitrogen adsorption−desorption isotherm, conforming to a mesoporous solid with a BET specific surface area of 625 $m^2\ g^{-1}$ and a total pore volume of 0.37 $cm^3\ g^{-1}$ (Figure 2, Table 1). Measurement of the isotherm for MCM-41-L2 revealed a lower nitrogen uptake, with the specific surface area and pore volume reduced to about 70% of the values seen for MCM-41. A further reduction to 50% was observed for MCM-41-L2/Ln. The average pore diameters decreased from 3.7 to 3.2 nm by the anchoring of the pyrazolylpyridine ligand and the inclusion of the lanthanide complexes.

Vibrational Spectroscopy and ab Initio Calculations. For the modified materials MCM-41-L2/Ln, the IR bands of the silica support are very strong and broad and consequently most of the bands due to the tethered species are not evident, with the exception of those in the range of 1300−1620 cm^{-1} and a weak band at 685 cm^{-1}. In contrast, the Raman spectra show most of the strong and medium bands due to the supported species. These are essentially unshifted as compared to the "free" ligand L2, and the complexes **1** and **2**. However, there are some changes that can be attributed to the formation of the desired supported species. Figure 3 compares the Raman spectrum of MCM-41-L2/Eu in the region 1420−1550 cm^{-1} with the sum of the Raman spectra of the starting materials MCM-41-L2 and

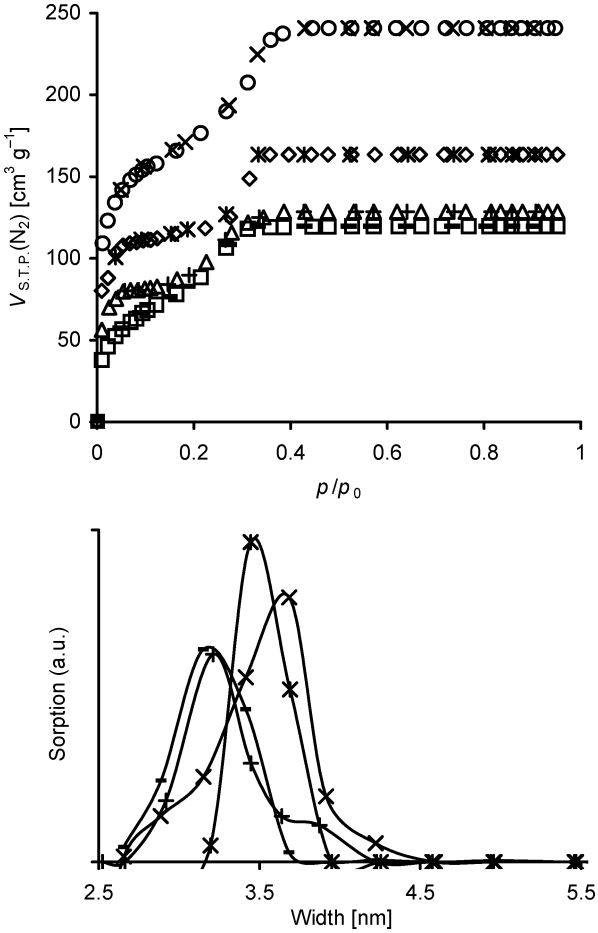

Figure 2. Nitrogen adsorption [MCM-41 (○), MCM-41-L2 (◇), MCM-41-L2/Eu (□), MCM-41-L2/Gd (△)] and desorption [MCM-41 (×), MCM-41-L2 (∗), MCM-41-L2/Eu (−), MCM-41-L2/Gd (+)] isotherms at 77 K, and pore size distributions (PSDs) of MCM-41 (×), MCM-41-L2 (∗), MCM-41-L2/Eu (−), and MCM-41-L2/Gd (+).

Table 1. Texture Parameters of MCM-41 Samples from N_2 Isotherms at 77 K

sample	S_{BET} [$m^2\ g^{-1}$]	ΔS_{BET}[a] (%)	V_t [$cm^3\ g^{-1}$]	ΔV_t[a] (%)	d_{BJH} [nm]
MCM-41	625		0.37		3.7
MCM-41-L2	450	−28	0.25	−32	3.4
MCM-41-L2/Eu	309	−51	0.18	−51	3.2
MCM-41-L2/Gd	326	−48	0.20	−46	3.2

[a] Variation of surface area and total pore volume in relation to parent MCM-41.

$Eu(NTA)_3{\cdot}2H_2O$. The bands at 1448 and 1505 cm^{-1} for the reagents are clearly affected by the inclusion process. These bands belong to the L2 fragment and have been assigned, based on ab initio calculations, to vibrational modes with dominant contributions from the C−N stretching of the pyrazole ring and to the inter-ring C−C stretching, respectively. These modes are expected to be highly affected by the coordination of the ligand to the lanthanide ions, especially considering the large structural reorganization of the free ligand required for complexation (Figure 4).

XAFS Spectroscopy. Eu L_3-edge XAFS spectra were measured in the solid state at room temperature for the compounds $Eu(NTA)_3{\cdot}2H_2O$, $Eu(NTA)_3{\cdot}$L1 (**1**), and MCM-41-L2/Eu. The normalized XANES data reveal single, intense edge resonances at 6.981 keV, in agreement with the Eu^{3+} reference compound $EuCl_3{\cdot}6H_2O$ (Figure 5). The absence

(23) (a) Marler, B.; Oberhagemann, U.; Voltmann, S.; Gies, H. *Microporous Mater.* **1996**, *6*, 375. (b) Hammond, W.; Prouzet, E.; Mahanti, S. D.; Pinnavaia, T. J. *Microporous Mesoporous Mater.* **1999**, *27*, 19.

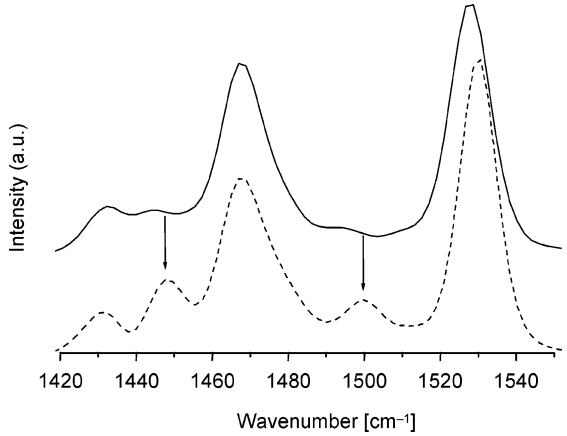

Figure 3. Raman spectrum of MCM-41-L2/Eu (−) in the range 1420−1550 cm^{-1} as compared to the sum of the spectra of the reagents MCM-41-L2 and $Eu(NTA)_3 \cdot 2H_2O$ (− − −). The most important changes are marked with an arrow.

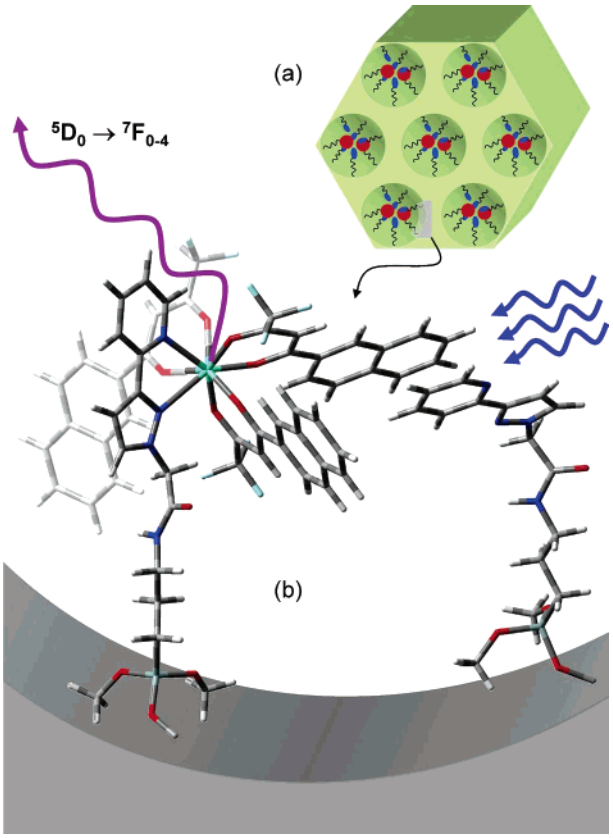

Figure 4. (a) Representation of MCM-41-L2/Eu showing the "free" pyrazolylpyridine ligands (blue ellipsoids) and europium tris-β-diketonate complexes (red circles) tethered to the channel walls. (b) Model of the intracavity assembling of europium complexes and free pyrazolylpyridine ligands (L2). Ab initio calculations at the B3LYP/LanL2DZ(N*) level reveal that the ligand L2 has to undergo a 180° rotation about the inter-ring C−C bond (with breaking of the intramolecular N−H···N hydrogen bond) to complex in a bidentate manner with the $Eu(NTA)_3$ fragment. Both complexes and free ligands can interact through a net of π−π stacking interactions, strong N−H···N and N−H···O hydrogen bonds, and weaker C−H···O and N−H···F contacts.

of any additional peaks shifted approximately 8 eV to the low energy side of the Eu^{3+} resonance confirms that the samples do not contain any divalent or intermediate-valent Eu.[24] For compounds **1** and MCM-41-L2/Eu, the amplitude and frequency of the oscillations on the high energy side of the Eu^{3+} resonance are identical, indicating very similar local

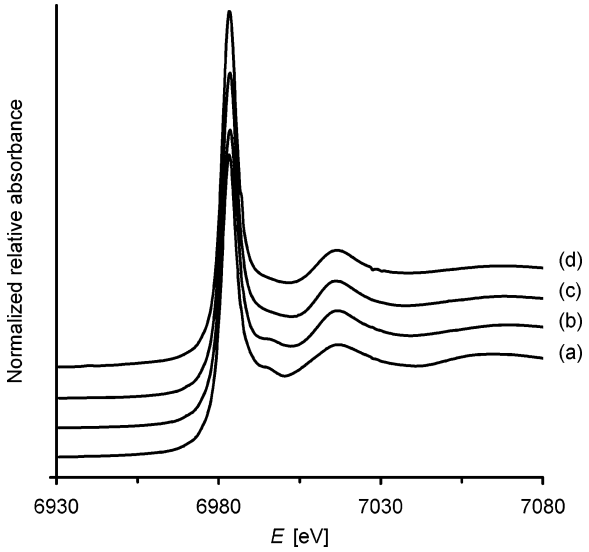

Figure 5. Eu L_3-edge XANES spectra of $EuCl_3 \cdot 6H_2O$ (a), $Eu(NTA)_3 \cdot 2H_2O$ (b), $Eu(NTA)_3 \cdot$L1 (**1**) (c), and MCM-41-L2/Eu (d).

Eu coordination environments. The spectra for $Eu(NTA)_3 \cdot 2H_2O$ and $EuCl_3 \cdot 6H_2O$ are slightly different in that there is a resolved shoulder at about 6.996 keV.

Figure 6 shows the Eu L_3-edge EXAFS spectra and corresponding Fourier transforms for the compounds $Eu(NTA)_3 \cdot 2H_2O$, $Eu(NTA)_3 \cdot$L1 (**1**), and MCM-41-L2/Eu. In each case, a two-shell model was used to fit the data, comprising 7−8 oxygen atoms at 2.38−2.39 Å and about 8 carbon atoms at 3.42−3.45 Å (Table 2). The Eu−O distance is in agreement with the single-crystal X-ray data for the adduct $Eu(NTA)_3 \cdot$phen.[5l] In this compound, the Eu atom is coordinated to the nitrogen atoms of the phenanthroline group with Eu−N = 2.584 and 2.586 Å, and to the oxygen atoms of three NTA groups, Eu−O = 2.348−2.395 Å. It is reasonable to assume that the Eu−O and Eu−N bond lengths for the H_2O and pyrazolylpyridine ligands in $Eu(NTA)_3 \cdot 2H_2O$ and **1** are approximately 0.2 Å longer than the Eu−O distances for the β-diketonate ligands. This difference is not sufficient to allow a separate shell to be fitted to the EXAFS data, and in fact the refined coordination numbers for the first shell indicate a contribution from the neutral ligands in addition to the six oxygen atoms of the NTA groups. The replacement of the H_2O ligands in $Eu(NTA)_3 \cdot 2H_2O$ by bidentate pyrazolylpyridine ligands cannot be confirmed by the EXAFS analysis alone, mainly due to the similarity of the backscattering amplitudes and phases for oxygen and nitrogen atoms. However, there is an obvious visual match between the EXAFS spectrum of MCM-41-L2/Eu and the model complex **1**. The second shell fitted to the Eu L_3-edge EXAFS of the three compounds corresponds mainly to the carbon atoms of the NTA CO groups [cf., 3.35 to 3.42 Å for $Eu(NTA)_3 \cdot$phen].

Photoluminescence Studies. Figure 7 shows the excitation spectra of $Eu(NTA)_3 \cdot$L1 (**1**) and the supported material MCM-41-L2/Eu monitored around the Eu^{3+} $^5D_0 \rightarrow {}^7F_2$ transition. The spectrum of **1** presents a large broad band

(24) Antonio, M. R.; Soderholm, L.; Jennings, G.; Francesconi, L. C.; Dankova, M.; Bartis, J. *J. Alloys Compd.* **1998**, *275−277*, 827 and references therein.

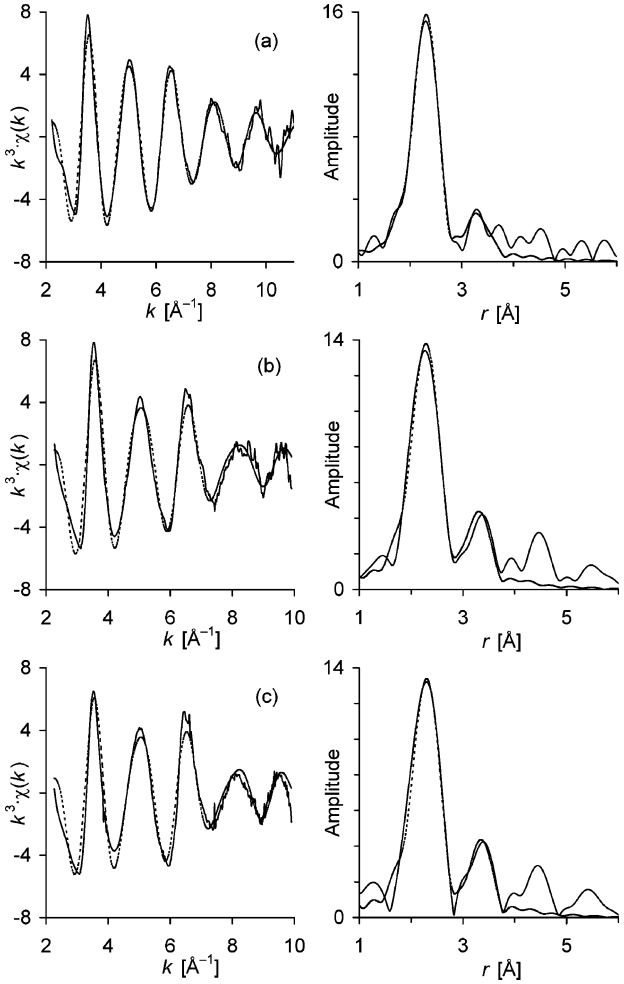

Figure 6. Eu L_3-edge EXAFS and Fourier transforms of $Eu(NTA)_3 \cdot 2H_2O$ (a), $Eu(NTA)_3 \cdot L1$ (**1**) (b), and MCM-41-L2/Eu (c). The solid line represents the experimental data, and the dashed line shows the best fit using parameters given in Table 2.

Table 2. Eu L_3-Edge EXAFS-Derived Structural Parameters for $Eu(NTA)_3 \cdot 2H_2O$, $Eu(NTA)_3 \cdot L1$ (1), and the Supported Material MCM-41-L2/Eu

compound	atom	CN[a]	r [Å]	$2\sigma^2$ [Å^2][b]	E_f [eV][c]	R (%)[d]
$Eu(NTA)_3 \cdot 2H_2O$	O	7.5(4)	2.388(4)	0.0189(8)	−7.9(3)	21.8
	C	8.0(20)	3.439(19)	0.0370(63)		
1	O	7.8(5)	2.379(6)	0.0251(24)	−6.9(4)	28.5
	C	8.5(17)	3.421(16)	0.0263(47)		
MCM-41-L2/Eu	O	7.0(5)	2.389(6)	0.0221(13)	−7.1(4)	29.1
	C	7.5(16)	3.452(16)	0.0212(44)		

[a] CN = coordination number. Values in parentheses are statistical errors generated in EXCURVE. The true errors in coordination numbers are likely to be of the order of 20%; those for the interatomic distances are ca. 1.5%.[25] [b] Debye−Waller factor; σ = root-mean-square internuclear separation. [c] E_f = edge position (Fermi energy), relative to calculated vacuum zero. [d] $R = (\int[\sum^{\text{theory}} - \sum^{\text{exptl}}]k^3\, dk / [\sum^{\text{exptl}}]k^3\, dk) \times 100\%$.

between 225 and 500 nm where it is possible to discern four main humps around 290, 325, 370, and 395 nm. This band superimposes a series of sharp lines characteristic of the Eu^{3+} energy level structure, assigned to the $^7F_0 \rightarrow {}^5D_{2,1}$ and $^7F_1 \rightarrow {}^5D_1$ transitions. For MCM-41-L2/Eu, a large broad band dominates the excitation spectrum and only a low intensity transition between the $^7F_0$ and the $^5D_2$ level can be discerned. This intensity decrease of the Eu^{3+} lines shows that the incorporation of the metal ion in the MCM host has

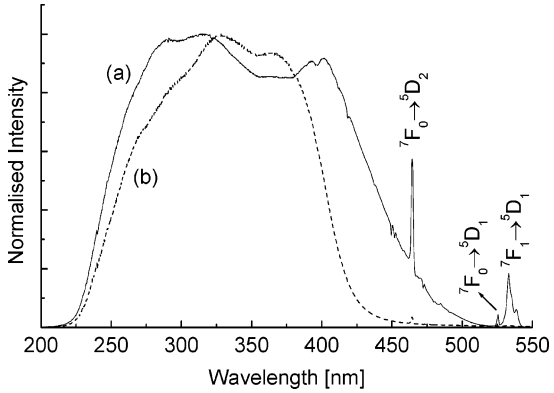

Figure 7. Room-temperature excitation spectra monitored at 611 nm of (a) $Eu(NTA)_3 \cdot L1$ (**1**) and (b) the supported material MCM-41-L2/Eu.

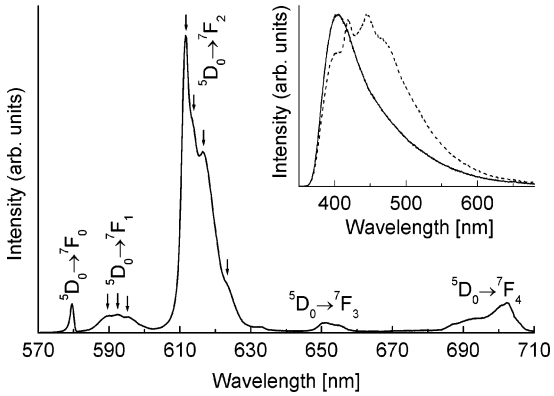

Figure 8. Room-temperature emission spectrum of MCM-41-L2/Eu excited at 325 nm. The inset shows the emission spectra of MCM-41-L2 excited at 325 nm at room temperature (−) and 12 K (− − −).

contributed to an increase of the Eu^{3+} sensitized process, when compared to the direct metal excitation. The excitation components may be related to excited states of the ligands or to ligand-to-metal charge-transfer (LMCT) transitions resulting from the interaction between the ion and the ligands in the Eu^{3+} first coordination shell. To verify the nature of these excitation bands, the diffuse reflectance spectra of Ln-$(NTA)_3 \cdot L1$ (**1**, **2**) and the supported materials MCM-41-L2/Ln (Ln = Eu, Gd) were recorded (not shown). The Eu complex **1** and MCM-41-L2/Eu show an absorption similar to that of the analogous Gd-based compounds, indicating that the absorption region is essentially due to transitions populating excited states localized in the ligands.

Figure 8 shows the room-temperature emission spectrum of MCM-41-L2/Eu under the excitation wavelength that maximizes the Eu^{3+} emission intensity. The spectrum is composed of the $^5D_0 \rightarrow {}^7F_{0-4}$ sharp lines typical of the Eu^{3+} energy level structure. The local-ligand field splitting is particularly evident for the $^5D_0 \rightarrow {}^7F_{1-2}$ transitions, presenting 3 and (at least) 4 Stark components, respectively (marked with arrows), suggesting that the Eu^{3+} ions occupy a low site symmetry group, without inversion center according to the higher intensity of the $^5D_0 \rightarrow {}^7F_2$ transition. The presence of only one line for the $^5D_0 \rightarrow {}^7F_0$ transition strongly indicates the existence of only one coordination site for the Eu^{3+} cations, as this transition occurs between nondegenerated levels. These emission features are identical to those found for the Eu^{3+} model compound $Eu(NTA)_3 \cdot L1$ (**1**), suggesting that the Eu^{3+} first coordination spheres are the same for both

(25) Evans, J.; Gauntlett, J. T.; Mosselmans, J. F. W. *Faraday Discuss. Chem. Soc.* **1990**, 107.

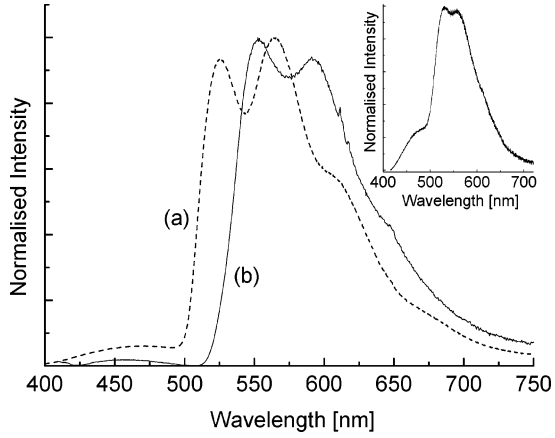

Figure 9. Emission spectra (10 K) of (a) MCM-41-L2/Gd and (b) Gd(NTA)$_3$·L1 (**2**) excited at 380 and 398 nm, respectively. The inset shows the room-temperature spectrum of MCM-41-L2/Gd excited at 390 nm.

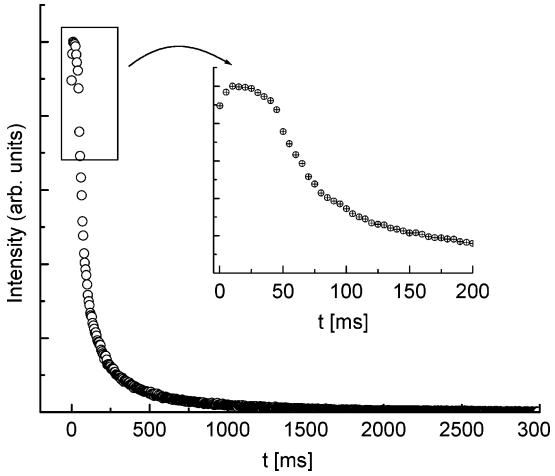

Figure 10. Experimental decay curve (12 K) for MCM-41-L2 excited at 325 nm and monitored at 420 nm.

compounds. No emission from the Eu^{3+}-ligands could be detected, which may be associated with an efficient ligands-to-Eu^{3+} energy transfer, because the Gd^{3+}-based compounds emit at room temperature (Figure 9).

The emission spectrum of MCM-41-L2/Gd displays three main peaks and a lower intensity one on the high energy side at ~455 nm (21 978 cm^{-1}). The three main peaks, which are centered around 525 nm (19 048 cm^{-1}), 563 nm (17 762 cm^{-1}), and 606 nm (16 502 cm^{-1}), may be ascribed to a resolvable vibrational fine structure originating from a single triplet (T_1) state. The spectrum of Gd(NTA)$_3$·L1 (**2**) is similar to that observed for MCM-41-L2/Gd but red-shifted in energy. There is a high energy component with the same energy as that found for MCM-41-L2/Gd, and three peaks centered around 553 nm (18 083 cm^{-1}), 594 nm (16 835 cm^{-1}), and 640 nm (15 625 cm^{-1}). The fact that the separation of the three main peaks for the two Gd compounds is in the range 1210−1286 cm^{-1}, which corresponds approximately to a vibrational progression typical of the n,π^* emission of aromatic molecules,[26] supports the former assignment. The decay curves for complex **2** and MCM-41-L2/Gd monitored at the lowest emission wavelength of the T_1 state (ca. 18 083 and 19 048 cm^{-1}, respectively) could be fitted by a single-exponential function leading to lifetime values of 1.85 ± 0.03 and 5.29 ± 0.05 ms, respectively, which are similar to those reported for other β-diketone ligands.[4] Such a long-lived emission further supports the triplet assignment.

Although a high number (66%) of free pyrazolylpyridine ligands exist in MCM-41-L2/Eu, no emission associated with these groups could be recorded, despite their efficient photoluminescence (12−300 K) in MCM-41-L2 (inset of Figure 8). This can be explained by considering an additional nonradiative deactivation channel for that ligand emission in MCM-41-L2/Eu and/or the occurrence of an unusual two-step intermolecular energy transfer between "free" ligands and complexed ligands followed by complexed ligands-to-Eu^{3+} ions.

The low-temperature emission spectrum of MCM-41-L2 consists of three main peaks centered at ca. 420, 445, and 471 nm, and a shoulder at ca. 405 nm. At room temperature, only the shoulder is evident (inset of Figure 8). The three main peaks are ascribed to a resolvable vibrational fine structure (the energy of which, 1374 ± 30 cm^{-1}, is typical of the n,π^* emission of aromatic molecules[26]) originating from a single triplet (T_1) state. The low-temperature decay curve of MCM-41-L2 monitored around the T_1 state (ca. 23 838 cm^{-1}, set as the lowest emission wavelength peak) reveals a nonexponential behavior with rise time character below 15 ms (Figure 10). This is further evidence for the existence of the first step of the above-mentioned energy transfer process between "free" and complexed ligands.

Table 3. Experimental $^5D_0$ Lifetime, Calculated Radiative and Nonradiative $^5D_0$ Decay Rates, Quantum Efficiency, and Radiance for Eu(NTA)$_3$·L1 (1) and the Supported Material MCM-41-L2/Eu

sample	τ [ms]	k_r [ms^{-1}]	k_{nr} [ms^{-1}]	q (%)	radiance [$\mu W/cm^2$]
Eu(NTA)$_3$·L1 (**1**)	0.637	0.831	0.739	52.9	0.73
MCM-41-L2/Eu	0.473	0.844	1.270	39.9	0.33

The lifetimes of the $^5D_0$ Eu^{3+} excited level (τ_{exp}) for MCM-41-L2/Eu and the Eu^{3+} model compound **1** were measured at room temperature using an excitation wavelength of 325 nm and monitored around the most intense emission line at 612 nm (not shown). All of the data are well fitted by a single-exponential function (Table 3), confirming that all lanthanide ions occupy the same average local environment within each sample. The lower value found for the $^5D_0$ lifetime of MCM-41-L2/Eu indicates that the nonradiative (k_{nr}) transition probability is higher, despite similar metal ion first coordination shells. To further investigate this point, the radiative transition probability (k_r), k_{nr}, and the efficiency, $q = k_r/(k_r + k_{nr})$, of the $^5D_0$ Eu^{3+} excited state were estimated using a procedure described elsewhere (Table 3).[2b,4,5f,l,m] An average index of refraction equal to 1.5 was considered for both compounds, giving $A(^5D_0 \rightarrow {}^7F_1) \approx 50$ s^{-1},[27] and in vacuo $A(^5D_0 \rightarrow {}^7F_1) = 14.65$ s^{-1}.[28] The q values were 53% for **1** and 40% for MCM-41-L2/Eu. The lower q value for the immobilized complex is due mainly to a higher k_{nr} parameter. This may be related to the energetic position of the Eu^{3+} intra-4f ^{6} levels with respect to the ligand triplet

(26) Ray, K.; Shanzer, A.; Waldeck, D. H.; Naaman, R. *Phys. Rev. B* **1999**, *60*, 13347.
(27) Hazenkamp, M. F.; Blasse, G. *Chem. Mater.* **1990**, *2*, 105.
(28) Werts, M. H. V.; Jukes, R. T. F.; Verhoeven, J. W. *Phys. Chem. Chem. Phys.* **2002**, *4*, 1542.

levels. The T_1 state of the ligands is closer to the $^5D_1$ level in the MCM-41-based sample. While a higher energy transfer rate is expected between the ligand and the Eu^{3+} cations as the $T_1-{}^5D_1$ energy transfer pathway is the channel with the higher energy transfer rate (due to dominance of the exchange mechanism),[29] a higher energy back-transfer rate might also occur, contributing to an increase in the k_{nr} parameter.

Another difference between the two Eu^{3+}-containing samples MCM-41-L2/Eu and $Eu(NTA)_3$·L1 (**1**) is the value of the radiance obtained under an excitation wavelength of 325 nm (Table 3). The radiance measurements for $Eu(NTA)_3$·L1 (**1**) and MCM-41-L2/Eu were performed under identical experimental conditions. Although the radiance for MCM-41-L2/Eu is about one-half of the value measured for the complex, the lower concentration of emitting centers in the MCM material (approximately 24 times lower than that in **1**) provides an effective radiance of more than 1 order of magnitude higher. Considering that the radiance depends on the excitation source (here, a 150 W Xe arc-lamp), the radiance of a commercial Eu^{3+} phosphor standard (Y_2O_3:Eu) with a quantum yield of 95% was measured under the same experimental conditions. The value obtained was 0.76 $\mu W/cm^2$, which is identical within experimental error (5%) to that found for the complex $Eu(NTA)_3$·L1 (**1**). This unequivocally places our materials at the level necessary for potential applications in the field of light emitters. Given that the $^5D_0$ quantum efficiency q for the supported complex is lower than that for **1**, the comparatively high radiance value for MCM-41-L2/Eu can only be explained by an increase in the population of the $^5D_0$ level (relative to that for **1**) due to an energy transfer mechanism, providing further evidence for the unusual two-step intermolecular energy transfer, that is, "free" pyrazolylpyridine ligands-to-complexed pyrazolylpyridine ligands-to-Eu^{3+} ions. Another fact supporting this energy transfer process is the energy of the T1 state for the coordinated ligands. Through the analyses of the isostructural MCM-41-L2/Gd samples (Figure 9), this energy was estimated to be ca. 19 048 cm^{-1}, approximately 4800 cm^{-1} below the energy measured for the free ligands in MCM-41-L2 (inset of Figure 8).

To interpret the exceptional photophysical behavior exhibited by the hybrid material MCM-41-L2/Eu, the intrapore arrangement of the tethered ligands/complexes needs to be considered in more detail. Elemental analysis for MCM-41-L2 indicated that the ligand content was 0.49 mmol g^{-1}. Taking into account the BET specific surface area of the original MCM-41 support, the surface coverage in MCM-41-L2 can be estimated as 0.57 molecules per nm^2; that is, the average surface area occupied by an anchored organic group is ca. 1.7 nm^2. It follows that the average separation of these groups is of the order of 1.3 nm. Obviously, the pyrazolylpyridine ligands will be closer together than this due to the curved nature of the MCM-41 channel walls. In fact, molecular modeling studies show that the anchored ligands and $Ln(NTA)_3$·L2 complexes may extend as far as 1.8 nm toward the center of the host channels, that is, nearly one-half of the average pore diameter of the original MCM-41 support determined from the nitrogen adsorption−desorption isotherm (Figure 4). The calculations also indicate that the area occupied by a tethered $Eu(NTA)_3$ complex is about 3 nm^2. Given that the europium content in MCM-41-L2/Eu was 0.13 mmol g^{-1}, we can further estimate that the total area occupied by immobilized complexes is 2.4×10^{20} $nm^2\ g^{-1}$, that is, 240 $m^2\ g^{-1}$. This is only slightly lower than the measured surface area of 309 $m^2\ g^{-1}$, suggesting that the tris-β-diketonate complexes are distributed quite closely together.

Conclusions

The complexes with the general formula $Ln(NTA)_3$·nL (Ln = Eu, Gd) are now known with L = H_2O, DMSO, 2,2′-bipyridine, 1,10-phenanthroline (phen), diazabutadiene (DAB), and pyrazolylpyridine (L1). Binuclear complexes of the type $[Ln(NTA)_3]_2$·bpym (bpym = 2,2′-bipyrimidine) have also been reported. The photoluminescence properties of these complexes vary considerably depending on the nature of L; for example, the $^5D_0$ quantum efficiencies (q) decrease in the order L = DMSO (62%), L1 (53%), phen (40%), bpym (39%), H_2O (29%), and DAB (2−3%). In the present work, complexes of the type $Ln(NTA)_3$·L have been successfully immobilized in the ordered mesoporous silica MCM-41 by complexation of the fragment $Ln(NTA)_3$ with a pyrazolylpyridine ligand covalently anchored to the support. A combination of vibrational spectroscopy and ab initio calculations, Eu L_3-edge XAFS, and photoluminescence spectroscopy confirm that the local coordination environment of the Eu^{3+} ions in the functionalized material is very similar to that in the model complex $Eu(NTA)_3$·L1 (**1**). Although the Eu-$(NTA)_3$ complexes are not spatially capable of coordinating with all of the pyrazolylpyridine ligands anchored to the MCM host, the effect of using a tethering procedure within the constrained environment of the host is that intermolecular interactions between the "free" ligands and supported complexes are promoted, thereby facilitating a nonradiative energy transfer process between interacting ligands. This type of intracavity assembling greatly enhances the antenna effect (when the ligands are partially engaged in coordination with Eu^{3+} ions), and therefore the lanthanide emission increases. The tethering procedure also means that the europium complexes are isolated from the siliceous support, thus minimizing any possible interactions with residual surface silanols that could lead to luminescence quenching. Moreover, the MCM-based material provides several additional advantages, such as being able to be processed as silica-based templates for optical centers (compatible with the silicon devices technology), opening up the possibility of designing new luminescent displays with highly oriented MCM-41 films impregnated with emitting centers showing enhanced antenna effects.

Acknowledgment. This work was supported by the FCT, POCTI, and FEDER (Project POCTI/CTM/46780/2002). We acknowledge the European Synchrotron Radiation Facility for provision of synchrotron radiation facilities and would like to thank Dr. Pier Lorenzo Solari for assistance in using beamline BM29. We also wish to thank Prof. João Rocha for generous support and access to research facilities.

(29) Silva, F. R. G.; Malta, O. L. *J. Alloys Compd.* **1997**, *250*, 427.

CM0514490